

1 **Forging new antibiotic combinations under iron-limiting conditions**

2 Derek C. K. Chan, Irene Guo, and Lori L. Burrows.

3 Department of Biochemistry and Biomedical Sciences, and the Michael G. DeGroot Institute for
4 Infectious Diseases Research, McMaster University, Hamilton, ON

5

6 **Running title: New thioStrepton-chelator combinations for *Pseudomonas* and *Acinetobacter***

7

8 **Keywords:** thioStrepton, iron, *Pseudomonas aeruginosa*, *Acinetobacter baumannii*

9

10 ***Correspondence to:**

11 Dr. Lori L. Burrows

12 2238 MDCL, 1280 Main St. West,

13 Hamilton, ON L8S 4L8 Canada

14 Tel: 905-525-9140 x 22029 Fax: 905-522-9033 Email: burrowl@mcmaster.ca

15 **ABSTRACT**

16 *Pseudomonas aeruginosa* is a multidrug-resistant nosocomial pathogen. We showed previously that
17 thioestrepton (TS), a gram-positive thiopeptide antibiotic, was imported via pyoverdine receptors and
18 synergized with iron chelator deferasirox (DSX) to inhibit the growth of *P. aeruginosa* and *Acinetobacter*
19 *baumannii* clinical isolates. A small number of *P. aeruginosa* and *A. baumannii* isolates were resistant to the
20 combination, prompting us to search for other compounds that could synergize with TS against those
21 strains. From literature surveys we selected 14 compounds reported to have iron-chelating activity, plus
22 one iron analogue, and tested them for synergy with TS. Doxycycline (DOXY), ciclopirox olamine (CO),
23 tropolone (TRO), clioquinol (CLI), and gallium nitrate (GN) synergized with TS. Individual compounds were
24 bacteriostatic but the combinations were bactericidal. Our spectrophotometric data and chrome azurol S
25 agar assay confirmed that the chelators potentiate TS activity through iron sequestration rather than
26 through their innate antimicrobial activities. A triple combination of TS + DSX + DOXY had the most potent
27 activity against *P. aeruginosa* and *A. baumannii* isolates. One *P. aeruginosa* clinical isolate was resistant to
28 the triple combination, but susceptible to a triple combination containing higher concentrations of CLI, CO,
29 or DOXY. All *A. baumannii* isolates were susceptible to the triple combinations. Our data reveal a diverse set
30 of compounds with dual activity as antibacterial agents and TS adjuvants, allowing combinations to be
31 tailored for resistant clinical isolates.

32

33 **INTRODUCTION**

34 Iron is a critical micronutrient for bacteria, influencing biofilm formation, pathogenicity, and growth (1, 2).
35 The opportunistic Gram-negative pathogen *Pseudomonas aeruginosa* has an extensive repertoire of iron
36 acquisition systems that are upregulated during iron-deplete conditions, similar to those encountered
37 during infection. To overcome iron limitation, *P. aeruginosa* produces the iron-scavenging siderophores
38 pyochelin and pyoverdine that bind iron with low and high affinity, respectively (3–5). Pyoverdine and its
39 outer membrane receptors, FpvA and FpvB, are highly expressed in low-iron conditions (3, 6, 7). Pyoverdine
40 has such a high binding affinity (10^{32} M^{-1}) for iron that it can strip it from transferrin, a mammalian protein
41 responsible for sequestering iron to impede bacterial growth (8–11). RNA-seq data showed that pyoverdine
42 biosynthetic enzymes and uptake are highly upregulated *in vivo* in response to the iron-deprived
43 environment (7). *P. aeruginosa* deficient in iron-uptake mechanisms are less able to cause infections
44 compared to their wild-type counterparts (12).

45

46 Natural products often exploit iron acquisition pathways to cross the Gram-negative outer membrane.
47 Pyocin S2, produced by *P. aeruginosa* to kill competing strains, and related toxins are taken up via FpvA (13,
48 14). The sideromycins, which resemble siderophores but have intrinsic antibacterial activity, also exploit
49 iron uptake pathways (15). Taking advantage of this phenomenon, several groups have created synthetic
50 siderophore-beta-lactam conjugates to target Gram-negative bacteria, using the iron-binding group as a
51 Trojan horse to deliver antibiotics (16–18). One such example is cefiderocol, a siderophore beta-lactam that
52 recently completed Phase III clinical trials. The catechol group of cefiderocol binds iron and the complex is
53 taken up via PiuA, an outer-membrane receptor for iron transport (18, 19). The compound demonstrated
54 potent activity against *Escherichia coli* and *Klebsiella pneumoniae* (19, 21). Thus, the Trojan horse approach
55 enhances the delivery of antibiotics compared to diffusion alone.

56
57 Our group recently discovered that the thiopeptide antibiotic thiostrepton (TS) hijacks pyoverdine receptors
58 under iron-limited conditions to cross the outer membranes of the World Health Organization's top two
59 critical priority pathogens, *P. aeruginosa* and *Acinetobacter baumannii* (22). TS activity was potentiated in
60 heat-inactivated mouse and human serum, and by FDA-approved iron chelators, deferiprone (DFP) and
61 deferasirox (DSX). However, a small number of *P. aeruginosa* and *A. baumannii* strains were resistant to TS-
62 chelator combinations, prompting us to look for new compounds that could synergize with TS to inhibit
63 those clinical isolates.

64
65 With the aim of finding compounds that could synergize with TS in iron-limiting conditions, we performed a
66 literature search to identify bioactive iron chelators. We selected 14 putative iron-binding compounds as
67 well as gallium, an iron analogue. Five compounds synergized with TS and had activity against *P. aeruginosa*
68 and *A. baumannii* clinical isolates. Each compound was bacteriostatic against *P. aeruginosa* PA14; however,
69 the addition of TS made the combination bactericidal. Growth of one highly-resistant *P. aeruginosa* clinical
70 isolate was inhibited with higher concentrations of three of the compounds in combination with TS+DSX.
71 These data identify a set of molecules of diverse structure and biological activity that synergize with TS,
72 providing the ability to tailor combinations for resistant strains.

73

74 **RESULTS**

75 **Iron-binding antibiotics form coloured complexes**

76 We first screened a panel of common antibiotics for potential iron-chelating activity using a qualitative
77 assay, monitoring change in colour upon addition of FeCl₃. Binding of transition metals results in formation

78 of coloured complexes that absorb in the visible wavelengths of light, detectable by spectroscopy and by
79 eye (23–25). The panel consisted of 22 antibiotics from the aminoglycoside, fluoroquinolone, beta-lactam,
80 and tetracycline classes (**Fig. 1**). Iron chelators DFP and DSX served as positive controls, turning dark
81 red/violet upon addition of ferric iron at a final concentration of 10 μ M. The tetracyclines – doxycycline
82 (DOXY), tetracycline, and minocycline – exhibited similar colour changes. The fluoroquinolones –
83 ciprofloxacin, ofloxacin, and piperidic acid – formed orange complexes; however, the intensity of the
84 colour change was weaker compared to the tetracyclines, DFP, and DSX. A number of beta-lactams showed
85 colour changes ranging from a brown-orange to red-orange. Ceftriaxone was the only beta-lactam that
86 turned red in the presence of ferric iron. Trimethoprim turned golden-yellow.

87

88 **Binding of ferric iron shifts absorption spectra**

89 To verify spectral shifts for compounds that changed colour upon addition of ferric iron, a 96-well
90 spectrophotometric assay was performed, with final concentrations of antibiotic and FeCl_3 of 300 μ M each.
91 The absorption spectra were scanned from 300 – 700 nm. The spectra of ciprofloxacin (CIP), piperidic acid,
92 ofloxacin, tetracycline, minocycline, DOXY, DSX and DFP shifted after the addition of FeCl_3 (**Fig. 2**),
93 confirming the results of the qualitative assay. Chloramphenicol and ampicillin served as negative controls.
94 The spectrum for ceftriaxone did not change at the concentrations tested, suggesting that the changes in
95 color observed for beta-lactams were likely due to concentration effects.

96

97 **Identification of other compounds that chelate iron**

98 To expand our panel of potential chelators beyond known antibiotics, we searched the literature for
99 bioactive compounds that were reported to have iron-chelating activity. We identified 14 compounds
100 (**Table 1**) plus gallium nitrate (GN). Gallium is an iron analogue that inhibits siderophore production, iron
101 uptake, and the activity of enzymes that use iron (26). The spectrophotometric assay was repeated for all
102 compounds listed in **Table 1** except for clioquinol (CLI). CLI was identified in our previous screen as a *P.*
103 *aeruginosa* growth inhibitor (22) but precipitated at concentrations above 8 μ g/mL. Ciclopirox olamine (CO)
104 and tropolone (TRO) showed shifts in their absorption spectra (**Fig. 2**). A chrome azurol S (CAS) assay was
105 also used to detect iron binding through de-colourization of the blue agar, indicating removal of Fe^{3+} from
106 the CAS-HDTMA complex (**Fig. S1**). DSX, TRO, and CO showed the greatest decolourization, and thus the
107 highest relative affinity for iron. Interestingly, DOXY showed a marked colour shift in the presence of Fe^{3+}
108 (**Fig. 2**) but minimally decolourized CAS agar.

109

110 **Numerous iron chelators synergize with TS**

111 Based on their ability to bind iron, each compound from Table 1, as well as DOXY and CIP, were assessed for
112 synergy with TS using checkerboard assays. DOXY, CO, CLI, TRO, and GN all synergized with TS (**Fig. 3**), as
113 IC₅₀ isobolograms showed that all combinations were below the line of additivity. Combination indices (CIs)
114 were less than 1 (**Fig. 3E**). Based on the checkerboards, isobolograms, and CI values, CO and CLI
115 demonstrated the most potent synergy with TS while GN had the weakest. Attempts to combine GN with
116 DSX or CO resulted in antagonism, likely due to the chelators binding Ga³⁺ (**Fig. S2**).

117

118 **Each compound potentiates TS activity**

119 We previously showed that iron chelation potentiated the effects of TS, as DSX alone had no anti-
120 *Pseudomonas* activity (22). CLI, TRO, DOXY, and CO can inhibit *P. aeruginosa* growth, suggesting that the
121 innate activity of the compounds could be partly responsible for synergy with TS. Thus, we considered four
122 potential mechanisms of synergy. 1) TS potentiates the activity of each compound through an unknown
123 mechanism. 2) The compound potentiates TS activity by chelating calcium and magnesium and increasing
124 outer membrane permeability or 3) by chelating iron and increasing TS uptake. In all these cases, the
125 synergy is unidirectional. 4) TS and the compound potentiate one another through an unknown mechanism.

126

127 Our data suggest that the synergy between TS and each compound is due to their iron chelation capacity
128 rather than membrane permeabilization. First, to determine if DOXY could increase outer membrane
129 permeability, vancomycin (VAN) and DOXY combinations were tested against PA14 alone or in the presence
130 of Ca²⁺, Mg²⁺ or Fe³⁺ (**Fig. S3**). VAN was selected because it is similar to TS in size but unlike TS, its activity is
131 unrelated to iron availability. VAN has a high minimal inhibitory concentration (MIC) against *P. aeruginosa*
132 due to limited uptake across the outer membrane. If a compound increases membrane permeability, we
133 expect synergy with VAN. In our checkerboard assays, no synergy was identified for VAN + DOXY, VAN + CLI,
134 VAN + CO, or VAN + TRO. Further, addition of 100 μM Mg²⁺ or Ca²⁺ had no effect on the checkerboard
135 profiles compared to control. In contrast, addition of 100 μM Fe³⁺ abrogated the inhibitory activity of CLI,
136 TRO, and CO, confirming that iron chelation is a critical part of the mechanism by which those compounds
137 impede growth. Lack of synergy between VAN + DOXY also suggested lack of membrane permeabilization.
138 The addition of 100 μM Mg²⁺ had no effect on the checkerboard whereas the addition of Fe³⁺ and Ca²⁺ had a
139 negligible effect. This is reflective of the relatively weak ability of DOXY to compete for iron in the CAS assay
140 (**Fig. S1**) and of its weak synergy with TS compared to other compounds.

141

142 To test the hypothesis that the compounds potentiate TS activity, rather than the other way around, 3D
143 checkerboard assays were performed using PA14. The surface area of each checkerboard was expressed as
144 % of control and graphed against the concentration of the third compound (**Fig. S4**). Individual MIC assays
145 for each compound were performed and the results graphed as % of control on the same y-axis on a log₁₀
146 scale. Significant differences between the two datasets would indicate that the TS + DSX combination
147 potentiates the activity of the test compound. To account for potential antagonism between test
148 compounds and DSX, 2D checkerboard assays were conducted (**Fig. S5**). DSX + TRO and DSX + CO were
149 indifferent. CLI antagonized with DSX at the MIC; however, we could not test concentrations of CLI greater
150 than 8 µg/mL due to its poor solubility. DSX was additive with DOXY. We saw no significant differences
151 between the activity of the chelators alone or in combination with TS and DSX, except for with CLI (**Fig.**
152 **4ABCD**). CLI antagonized DSX at the highest concentration; however, growth was still below 20% of control
153 (**Fig. 4C**), which we previously established as equivalent to the MIC in the growth medium used for this work
154 (22). When the data were plotted against TS concentration (**Fig. 4E**), significant differences for the
155 combinations were apparent at 2 and 4 µg/mL TS compared to TS alone, indicating that the compounds and
156 DSX potentiate TS activity. These data suggest that the synergy between the chelators and TS is
157 unidirectional.

158

159 **TS combinations are bactericidal and effective against clinical isolates**

160 TS, CO, CLI, DOXY, and TRO alone were bacteriostatic; however, when combined with TS, the combinations
161 were bactericidal (**Fig. S6**). This improved activity prompted us to test the combinations against clinical
162 isolates. Double (TS + compound) and triple combinations (TS + DSX + compound) were tested against same
163 panels of *P. aeruginosa* and *A. baumannii* clinical isolates we previously assayed for susceptibility to TS +
164 DSX (**Fig. 5**) (22). GN was omitted due to its weak synergy with TS against PA14 and antagonism with iron
165 chelators (**Fig. S2**). TS and DSX were used at 8.3 µg/mL (5 µM) and 32 µg/mL as before, while the other
166 compounds were added at 1/8th the MIC of PA14, corresponding to DOXY, CO, TRO, and CLI concentrations
167 of 1 µg/mL, 2 µg/mL, 4 µg/mL, and 1 µg/mL, respectively.

168

169 Of the double combinations, TS + DSX was the most potent against *P. aeruginosa* (**Fig. 5A**), consistent with
170 our checkerboard assays. Interestingly, TS + DOXY and TS + CO had similar potency despite differences in
171 their CI values (**Fig. 3**). TS + TRO was the least potent of the double combinations. TS + CLI potency was
172 similar to TS + DSX, and this combination reduced growth of our most resistant clinical isolate, C0379, while
173 TS + DSX did not. TS synergized with CLI to inhibit C0379 although a higher concentration (8 µg/mL) of CLI

174 was required (**Fig. 6**). Of the triple combinations, TS + DSX + DOXY was the most potent, with only C0379
175 showing resistance. We previously reported that C0379 has a partial deletion of *fvpB*, encoding a
176 pyoverdine receptor (22). However, triple combinations with higher concentrations of DOXY and CO could
177 inhibit its growth (**Fig. 6AC**). C0379 growth was also inhibited by TS + CLI or TS + DSX + CLI, if CLI was used at
178 8 µg/mL. CLI alone did not reduce growth below MIC and there was no antagonism between DSX and CLI
179 with C0379 compared to PA14 (**Fig. 6B**). C0379 was also less susceptible to TRO compared to PA14 (**Fig. 6D**).

180
181 For *A. baumannii* isolates, all double combinations were equally effective. TS + CLI was highly potent against
182 *A. baumannii* compared to *P. aeruginosa* when CLI was used at 1 µg/mL (**Figs. 5B and S7**). Strain C0286 was
183 resistant to TS but susceptible to TS + CLI, suggesting inhibition was due to CLI. Conversely, TS + TRO had
184 little activity against *P. aeruginosa* clinical isolates but was effective against *A. baumannii*. The triple
185 combinations inhibited the growth of both species.

186

187 DISCUSSION

188 A diverse repertoire of iron-uptake mechanisms allows *P. aeruginosa* to proliferate under iron-limited
189 conditions, similar to those encountered during infection of a host. Thus, repurposing iron chelators as
190 antibiotic adjuvants may increase expression of iron-uptake pathways that can then be exploited to deliver
191 antibacterial compounds. Both *P. aeruginosa* and *A. baumannii* express pyoverdine receptors FpvA and
192 FpvB, which are highly upregulated under iron-limited conditions (6, 7). TS hijacks these pyoverdine
193 receptors to enter the cell, as mutants lacking both receptors are resistant. The combination of TS + DSX
194 inhibited the growth of most clinical isolates (22). Here we identified additional iron-chelating compounds
195 that synergize with TS to inhibit growth of the few clinical isolates that were resistant to TS + DSX.

196

197 Antimicrobial-iron chelator combinations have been explored for treatment of both bacterial and fungal
198 infections. A combination of DSX and tobramycin inhibited *P. aeruginosa* biofilm formation on CF airway
199 cells (27), while chelation of iron by DOXY potentiated the activity of fluconazole against *Candida albicans*
200 (28). For *P. aeruginosa*, iron restriction has the added benefit of increasing twitching motility and reducing
201 biofilm formation, leaving cells more susceptible to antibiotic treatment (29).

202

203 Here we identified multiple compounds that synergize with TS against *P. aeruginosa* and *A. baumannii*
204 clinical isolates, due to their ability to chelate iron. Iron-binding capacity was demonstrated by monitoring
205 visual color changes when complexed with Fe³⁺, CAS agar decolorization, and via spectrophotometric

206 assays. The CAS assay, which is used to detect siderophore production, not only indicates whether a
207 compound can bind iron, but also if it has a stronger affinity for the metal than the CAS-HDTMA complex.
208 This allowed us to compare the relative binding affinities of various compounds based on the extent of
209 decolourization. This method is limited by compound solubility, as seen with CLI (**Fig. S1**).

210
211 None of the natural phytochelators from plants that we tested – including baicalin, ferulic acid, sodium
212 phytate, 2,3,5,6-tetramethylpyrazine, curcumin, epigallocatechin gallate, and phloretin (**Table 1**) – synergized
213 with TS. *P. aeruginosa* can act as a plant pathogen and may have evolved to outcompete or even take up
214 phytochelators (30–33). The compounds that synergized with TS are all synthetic and the extent of synergy
215 correlated with their ability to strip iron from CAS-Fe³⁺-HDTMA complexes (**Fig. 3 and Fig. S1**). Iron chelators
216 compete with siderophores and reduce iron availability, resulting in increased pyoverdine receptor
217 expression and susceptibility to TS (34). Weaker chelators such as DOXY and CIP showed little or no synergy
218 with TS whereas strong chelators like CO and TRO exhibited greater synergy.

219
220 The GN data demonstrate that synergy with TS can occur via routes other than iron chelation. Ga³⁺
221 represses pyoverdine production and forms complexes with pyoverdine that prevents iron binding (35, 36).
222 TS activity could be weakly potentiated because of reduced competition for pyoverdine receptors if
223 siderophore production decreases upon GN treatment. These data show that disrupting iron acquisition
224 may be another avenue for novel TS combinations. GN in triple combinations with TS + chelator has limited
225 utility because iron chelators bind Ga³⁺ (**Fig. S2**). However, one study showed that LK11, a compound that
226 inhibits pyoverdine function directly, sensitized cells to CO to the same extent as a pyoverdine null mutant
227 (37). Our previous work showed that a PA14 *pvdA* transposon mutant was more susceptible to TS compared
228 to the wild type, which suggests that pyoverdine biosynthesis inhibitors could be useful TS adjuvants (22).

229
230 In summary, TS synergizes with iron-chelating compounds of diverse structure that were not primarily
231 intended as antibacterial compounds. Although the mechanisms of action for some of these molecules are
232 not fully understood, they may reveal new targets for antibiotic therapy. In addition, TS combinations
233 demonstrated bactericidal activity while chelator compounds alone were bacteriostatic. The new
234 combinations were effective against clinical isolates resistant to TS+DSX. Our data suggests that these
235 compounds have dual roles – as antibacterial agents and TS adjuvants. Iron restriction mimics many *in vivo*
236 conditions, as host proteins sequester free iron in an attempt to starve bacteria and exert antibacterial

237 activity. Screening for antibiotic activity under similar conditions is an important strategy for development
238 of new treatments for the most dangerous pathogens.

239

240 **ACKNOWLEDGEMENTS**

241 We thank Gerry Wright for access to strains from the Wright Clinical Collection and Jakob Magolan for
242 synthesis of DSX. This work was funded by grants to LLB from the Natural Sciences and Engineering
243 Research Council (NSERC) RGPIN-2016-06521 and the Ontario Research Fund RE07-048. DC holds an NSERC
244 Canadian Graduate Scholarship – Master’s Award. IG held a Summer Studentship from Cystic Fibrosis
245 Canada.

246

247 **METHODS**

248 **Bacterial strains, compounds, and culture conditions**

249 *P. aeruginosa* PA14 was used for checkerboard assays as previously described (22). All clinical isolates were
250 from the Wright Clinical Collection as described previously. Bacteria overnight cultures were grown in
251 lysogeny broth (LB) and subcultured in 10:90 medium (10% LB, 90% phosphate buffered saline (PBS)). All
252 growth assays were done using 10:90 and grown for 16h at 37°C and 200 rpm. Compounds from Table 1
253 were from AK Scientific, Sigma, and Cayman Chemicals. TS and DSX were from Cayman Chemicals and AK
254 Scientific respectively. Compounds were stored at -20°C. Stock solutions were stored at -20°C until use
255 except for the tetracyclines, which were made fresh due to precipitation at -20°C.

256

257 **Absorption spectra assays for iron chelation**

258 Compounds were arrayed in Nunc 96 microwell plates. Vehicle controls contained Milli-Q H₂O with 1:75
259 dilution of each compound at a final concentration of 300µM. The experimental set-up contained the same
260 components as the vehicle control, with the addition of 300µM FeCl₃. The final volume in each well was
261 150µL. The plate was incubated at room temperature for one hour and absorption spectra from 300 nm to
262 700 nm was read in 2nm increments (Multiskan Go - Thermo Fisher Scientific).

263

264 **CAS assay**

265 CAS agar plates were prepared as described previously (22). Compounds were standardized to 2 mg/mL and
266 10 µL of each was spotted onto the plate. Plates were incubated at room temperature for 1 h, then
267 photographed. Three replicates were conducted and the image of a representative plate was presented.

268

269 **Dose response and checkerboard assays**

270 Dose response and checkerboard assays were conducted as described previously (22). Briefly, overnight
271 cultures were grown in LB for 16 h, 37°C, 200 rpm then subcultured (1:500 dilution) into 10:90 for 6 h.
272 Subcultures were standardized to OD₆₀₀ of 0.10 and diluted 1:500 in fresh 10:90 before use. For the dose
273 response assay, serial dilutions of compounds were added at 75 times the final concentration and diluted
274 with 10:90 with cells to reach the desired final concentration. This was done in triplicate for technical
275 replicates. Vehicle and sterile controls were included. The checkerboard assay was done similarly to the
276 dose response assay but in an 8 x 8 format in a 96-well Nunc plate, with concentration of one drug
277 increasing along the y-axis and the other along the x-axis. Sterility and vehicle controls were included with
278 two columns allocated for each control. At least three biological replicates were repeated for the dose
279 response and checkerboard assays.

280

281 **3D Checkerboard Assays**

282 Three-dimensional checkerboard assays were performed in Nunc 96 microwell plates in an 8 x 8 x 8 matrix
283 format for a total of 512 wells. The first two columns were used for the vehicle controls while the last two
284 columns were allocated to sterility controls, both consisting of 2.7% (v/v) DMSO + 1.3% (v/v) H₂O for plates
285 with TRO and DOXY and 4% (v/v) DMSO for plates with CLI and CO. Serial dilutions of TS were added along
286 the y-axis of each plate starting at 0 µg/mL, with the highest final concentration being 4 µg/mL. Serial
287 dilutions of DSX were added along the x-axis of each plate, from 0 µg/mL to the highest final concentration
288 of 8 µg/mL. Serial dilutions of compound were added with an increasing concentration in each plate up to a
289 final concentration of 35 µg/mL (TRO), 8 µg/mL (DOXY), 30 µg/mL (CO), and 8 µg/mL (CLI) in the last plate.
290 Each well contained 144 µL of 10:90 inoculated with PA14, except for the sterility control columns which
291 contained 10:90 only. The final volume in each plate was 150 µL. The plates were sealed with parafilm and
292 incubated at 37°C for 16 h, shaking at 200 rpm. The OD₆₀₀ of the plates was read (Multiskan Go - Thermo
293 Fisher Scientific). Each experiment was repeated at least three times. Checkerboards were analyzed in
294 Excel. Representative plots at ¼ MIC were made using MATLAB. Surface areas were averaged, expressed in
295 % of control, and plotted against each compound concentration (Prism, Graphpad).

296

297 **Clinical Isolate Testing**

298 Isolates from the Wright Clinical Collection were grown and tested as described previously (22). Briefly,
299 clinical isolates were inoculated from glycerol stocks stored at -80°C into Nunc 96-well plates and grown
300 overnight at 37°C, for 16 h with shaking in LB (200 rpm). Overnights were subcultured (1:25) into fresh

301 10:90 medium and grown for 2 h under the same growth conditions. Subcultures were diluted 1:75 in fresh
302 10:90. Compounds were diluted 1:75 to obtain the final concentration. DOXY and CLI were added at a final
303 concentration of 1 µg/mL, CO was used at 2 µg/mL, TRO was used at 4 µg/mL, TS was used at 8.3 µg/mL,
304 and DSX was used at 32 µg/mL. Vehicle and sterility controls were included. Plates were incubated
305 overnight with the same conditions. The OD₆₀₀ was read (Multiscan Go – Thermo Fisher Scientific), analyzed
306 using Excel, and the data plotted using Prism (GraphPad).

307

308 REFERENCES

- 309 1. Banin E, Vasil ML, Greenberg EP. 2005. From The Cover: Iron and *Pseudomonas aeruginosa* biofilm
310 formation. *Proc Natl Acad Sci* 102:11076–11081.
- 311 2. Schaible UE, Kaufmann SHE. 2004. Iron and microbial infection. *Nat Rev Microbiol* 2:946–953.
- 312 3. Voulhoux R, Filloux A, Schalk IJ. 2006. Pyoverdine-mediated iron uptake in *Pseudomonas aeruginosa*:
313 the Tat system is required for PvdN but not for FpvA transport. *J Bacteriol* 188:3317–23.
- 314 4. Heinrichs DE, Young L, Poole K. 1991. Pyochelin-mediated iron transport in *Pseudomonas*
315 *aeruginosa*: Involvement of a high-molecular-mass outer membrane protein. *Infect Immun* 59:3680–
316 3684.
- 317 5. Cornelis P, Matthijs S, Van Oeffelen L. 2009. Iron uptake regulation in *Pseudomonas aeruginosa*, p.
318 15–22. *In BioMetals*.
- 319 6. Gonzalez MR, Ducret V, Leoni S, Fleuchot B, Jafari P, Raffoul W, Applegate LA, Que Y-A, Perron K.
320 2018. Transcriptome Analysis of *Pseudomonas aeruginosa* Cultured in Human Burn Wound
321 Exudates. *Front Cell Infect Microbiol* 8:39.
- 322 7. Damron FH, Oglesby-Sherrouse AG, Wilks A, Barbier M. 2016. Dual-seq transcriptomics reveals the
323 battle for iron during *Pseudomonas aeruginosa* acute murine pneumonia. *Sci Rep* 6:39172.
- 324 8. Ratledge C, Dover LG. 2000. Iron Metabolism in Pathogenic Bacteria. *Annu Rev Microbiol* 54:881–
325 941.
- 326 9. Meyer JM, Neely A, Stintzi A, Georges C, Holder IA. 1996. Pyoverdine is essential for virulence of
327 *Pseudomonas aeruginosa*. *Infect Immun* 64:518–23.
- 328 10. Eckenroth BE, Steere AN, Chasteen ND, Everse SJ, Mason AB. 2011. How the binding of human

- 329 transferrin primes the transferrin receptor potentiating iron release at endosomal pH. Proc Natl
330 Acad Sci U S A 108:13089–94.
- 331 11. Kang D, Kirienko N V. 2017. High-Throughput Genetic Screen Reveals that Early Attachment and
332 Biofilm Formation Are Necessary for Full Pyoverdine Production by *Pseudomonas aeruginosa*. Front
333 Microbiol 8:1707.
- 334 12. Minandri F, Imperi F, Frangipani E, Bonchi C, Visaggio D, Facchini M, Pasquali P, Bragonzi A, Visca P.
335 2016. Role of iron uptake systems in *Pseudomonas aeruginosa* virulence and airway infection. Infect
336 Immun 84:2324–2335.
- 337 13. Denayer S, Matthijs S, Cornelis P. 2007. Pyocin S2 (Sa) Kills *Pseudomonas aeruginosa* Strains via the
338 FpvA Type I Ferripyoverdine Receptor †. J Bacteriol 189:7663–7668.
- 339 14. Elfarash A, Wei Q, Cornelis P. 2012. The soluble pyocins S2 and S4 from *Pseudomonas aeruginosa*
340 bind to the same FpvAI receptor. Microbiologyopen 1:268–75.
- 341 15. Mislin GLA, Schalk IJ. 2016. Fluorescent Aliphatic Hyperbranched Polyether: chromophores-free and
342 without any N and P Atoms. Phys Chem Chem Phys 00:1–3.
- 343 16. Wittmann S, Schnabelrauch M, Scherlitz-Hofmann I, Möllmann U, Ankel-Fuchs D, Heinisch L. 2002.
344 New synthetic siderophores and their beta-lactam conjugates based on diamino acids and
345 dipeptides. Bioorg Med Chem 10:1659–70.
- 346 17. Kline T, Fromhold M, McKennon TE, Cai S, Treiberg J, Ihle N, Sherman D, Schwan W, Hickey MJ,
347 Warrenner P, Witte PR, Brody LL, Goltry L, Barker LM, Anderson SU, Tanaka SK, Shawar RM, Nguyen
348 LY, Langhorne M, Bigelow A, Embuscado L, Naeemi E. 2000. Antimicrobial effects of novel
349 siderophores linked to beta-lactam antibiotics. Bioorg Med Chem 8:73–93.
- 350 18. Brochu A, Brochu N, Nicas TI, Parr TR, Minnick AA, Dolence EK, McKee JA, Miller MJ, Lavoie MC,
351 Malouin F. 1992. Modes of action and inhibitory activities of new siderophore-beta-lactam
352 conjugates that use specific iron uptake pathways for entry into bacteria. Antimicrob Agents
353 Chemother 36:2166–75.
- 354 19. Ito A, Sato T, Ota M, Takemura M, Nishikawa T, Toba S, Kohira N, Miyagawa S, Ishibashi N,
355 Matsumoto S, Nakamura R, Tsuji M, Yamano Y. 2018. In vitro antibacterial properties of cefiderocol,
356 a novel siderophore cephalosporin, against gram-negative bacteria. Antimicrob Agents Chemother

- 357 62.
- 358 20. Ito A, Nishikawa T, Matsumoto S, Yoshizawa H, Sato T, Nakamura R, Tsuji M, Yamano Y. 2016.
359 Siderophore cephalosporin cefiderocol utilizes ferric iron transporter systems for antibacterial
360 activity against *Pseudomonas aeruginosa*. *Antimicrob Agents Chemother* 60:7396–7401.
- 361 21. Dobias J, Déneraud-Tendon V, Poirel L, Nordmann P. 2017. Activity of the novel siderophore
362 cephalosporin cefiderocol against multidrug-resistant Gram-negative pathogens. *Eur J Clin Microbiol*
363 *Infect Dis* 36:2319–2327.
- 364 22. Ranieri MRM, Chan DCK, Yaeger LN, Rudolph M, Karabelas-Pittman S, Abdo H, Chee J, Harvey H,
365 Nguyen U, Burrows LL. 2019. Thiostrepton hijacks pyoverdine receptors to inhibit growth of
366 *Pseudomonas aeruginosa*. *Antimicrob Agents Chemother* AAC.00472-19.
- 367 23. Petit L, Adamo C, Russo N. 2005. Absorption spectra of first-row transition metal complexes of
368 bacteriochlorins: A theoretical analysis. *J Phys Chem B* 109:12214–12221.
- 369 24. Sever MJ, Wilker JJ. 2004. Visible absorption spectra of metal–catecholate and metal–tironate
370 complexes. *J Chem Soc Dalton Trans* 4:1061–1072.
- 371 25. Sutton D. 2007. Electronic Spectra of Transition Metal Complexes. *J Electrochem Soc* 116:310C.
- 372 26. Kaneko Y, Thoendel M, Olakanmi O, Britigan BE, Singh PK. 2007. The transition metal gallium
373 disrupts *Pseudomonas aeruginosa* iron metabolism and has antimicrobial and antibiofilm activity. *J*
374 *Clin Invest* 117:877–88.
- 375 27. Moreau-Marquis S, O’Toole GA, Stanton BA. 2009. Tobramycin and FDA-approved iron chelators
376 eliminate *Pseudomonas aeruginosa* biofilms on cystic fibrosis cells. *Am J Respir Cell Mol Biol* 41:305–
377 313.
- 378 28. Fiori A, Van Dijck P. 2012. Potent synergistic effect of doxycycline with fluconazole against *Candida*
379 *albicans* is mediated by interference with iron homeostasis. *Antimicrob Agents Chemother* 56:3785–
380 3796.
- 381 29. Singh PK, Parsek MR, Greenberg EP, Welsh MJ. 2002. A component of innate immunity prevents
382 bacterial biofilm development. *Nature* 417:552–555.
- 383 30. Starkey M, Rahme LG. 2009. Modeling *Pseudomonas aeruginosa* pathogenesis in plant hosts. *Nat*

- 384 Protoc 4:117–124.
- 385 31. Rahme LG, Tan MW, Le L, Wong SM, Tompkins RG, Calderwood SB, Ausubel FM. 1997. Use of model
386 plant hosts to identify *Pseudomonas aeruginosa* virulence factors. Proc Natl Acad Sci U S A
387 94:13245–13250.
- 388 32. Green SK, Schroth MN, Cho JJ, Kominos SK, Vitanza-jack VB. 1974. Agricultural plants and soil as a
389 reservoir for *Pseudomonas aeruginosa*. Appl Microbiol 28:987–91.
- 390 33. Gi M, Lee K-M, Kim SC, Yoon J-H, Yoon SS, Choi JY. 2015. A novel siderophore system is essential for
391 the growth of *Pseudomonas aeruginosa* in airway mucus. Sci Rep 5:14644.
- 392 34. Smith DJ, Lamont IL, Anderson GJ, Reid DW. 2013. Targeting iron uptake to control *Pseudomonas*
393 *aeruginosa* infections in cystic fibrosis. Eur Respir J.
- 394 35. Kaneko Y, Thoendel M, Olakanmi O, Britigan BE, Singh PK. 2007. The transition metal gallium
395 disrupts *Pseudomonas aeruginosa* iron metabolism and has antimicrobial and antibiofilm activity. J
396 Clin Invest 117:877–88.
- 397 36. Ross-Gillespie A, Weigert M, Brown SP, Kümmerli R. 2014. Gallium-mediated siderophore quenching
398 as an evolutionarily robust antibacterial treatment. Evol Med Public Heal 2014:18–29.
- 399 37. Kirienko DR, Kang D, Kirienko N V. 2018. Novel Pyoverdine Inhibitors Mitigate *Pseudomonas*
400 *aeruginosa* Pathogenesis. Front Microbiol 9:3317.
- 401 38. Perez CA, Wei Y, Guo M. 2009. Iron-binding and anti-Fenton properties of baicalein and baicalin. J
402 Inorg Biochem 103:326–332.
- 403 39. Zhang Y, Li H, Zhao Y, Gao Z. 2006. Dietary supplementation of baicalin and quercetin attenuates
404 iron overload induced mouse liver injury. Eur J Pharmacol 535:263–269.
- 405 40. Zhao Y, Li H, Gao Z, Xu H. 2005. Effects of dietary baicalin supplementation on iron overload-induced
406 mouse liver oxidative injury. Eur J Pharmacol 509:195–200.
- 407 41. Hatcher HC, Singh RN, Torti FM, Torti S V. 2009. Synthetic and natural iron chelators: Therapeutic
408 potential and clinical use. Future Med Chem 1:1643-1670
- 409 42. Hynes MJ, Ó Coinceanainn M. 2002. Investigation of the release of iron from ferritin by naturally

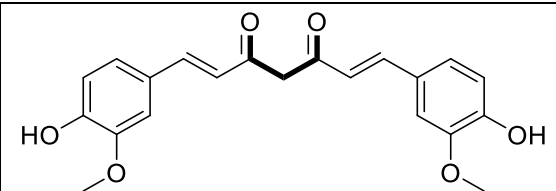
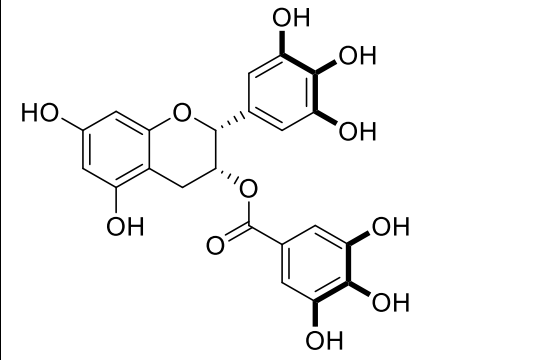
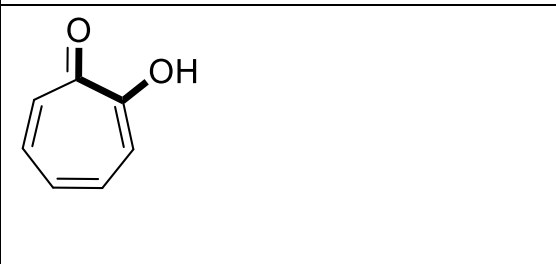
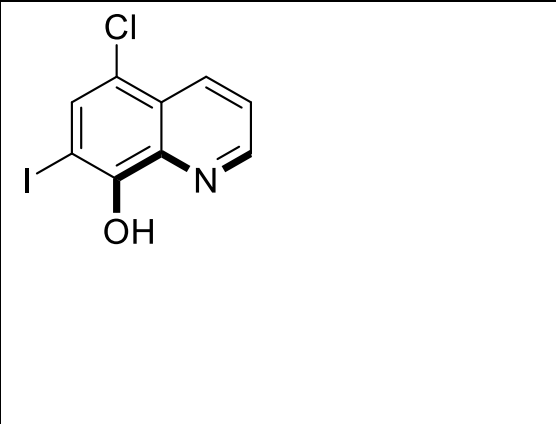
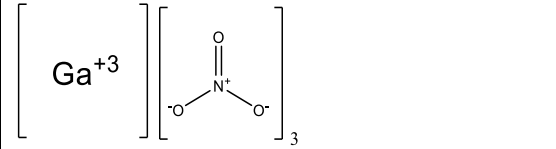
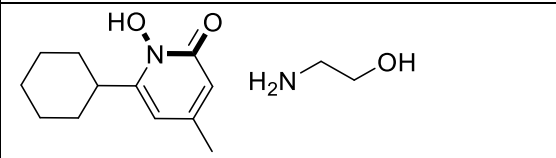
- 410 occurring antioxidants. *J Inorg Biochem* 90:18–21.
- 411 43. Boyer RF, Clark HM, LaRoche AP. 1988. Reduction and Release of Ferritin Iron By Plant Phenolics. *J*
412 *Inorg Biochem* 32:171–181.
- 413 44. Xu Q, Kanthasamy AG, Reddy MB. 2008. Neuroprotective effect of the natural iron chelator, phytic
414 acid in a cell culture model of Parkinson’s disease. *Toxicology* 245:101–108.
- 415 45. Minihane AM, Rimbach G. 2002. Iron absorption and the iron binding and anti-oxidant properties of
416 phytic acid. *Int J Food Sci Technol* 37:741–748.
- 417 46. Kamp DW, Israbian VA, Panos RJ, Yeldandi A V, Graceffa P, Weitzman SA. 1995. Phytic Acid, an Iron
418 Chelator, Attenuates Pulmonary Inflammation and Fibrosis in Rats after Intratracheal Instillation of
419 Asbestos. *Toxicol Pathol* 23:689–695.
- 420 47. Kock ND, Torti S V, Knovich MA, D’Agostino R, Wilkinson J, Jiao Y, Hatcher H, Torti FM, Di X, Wang W.
421 2008. Curcumin, a cancer chemopreventive and chemotherapeutic agent, is a biologically active iron
422 chelator. *Blood* 113:462–469.
- 423 48. Baum L, Ng A. 2004. Curcumin interaction with copper and iron suggests one possible mechanism of
424 action in Alzheimer’s disease animal models. *J Alzheimer’s Dis* 6:367–377.
- 425 49. Weinreb O, Amit T, Mandel S, Youdim MBH. 2009. Neuroprotective molecular mechanisms of (-)-
426 epigallocatechin-3-gallate: A reflective outcome of its antioxidant, iron chelating and neuritogenic
427 properties. *Genes Nutr. BioMed Central*.
- 428 50. Mandel SA, Amit T, Kalfon L, Reznichenko L, Weinreb O, Youdim MBH. 2008. Cell signaling pathways
429 and iron chelation in the neurorestorative activity of green tea polyphenols: Special reference to
430 epigallocatechin gallate (EGCG). *J Alzheimer’s Dis. IOS Press*.
- 431 51. Higuchi A, Yonemitsu K, Koreeda A, Tsunenari S. 2003. Inhibitory activity of epigallocatechin gallate
432 (EGCg) in paraquat-induced microsomal lipid peroxidation - A mechanism of protective effects of
433 EGCg against paraquat toxicity. *Toxicology* 183:143–149.
- 434 52. Azegami K, Nishiyama K, Kato H. 1988. Effect of iron limitation on *Pseudomonas plantarii* growth and
435 tropolone and protein production. *Appl Environ Microbiol* 54:844–847.
- 436 53. Ganeshaguru K, Hoffbrand AV, Grady RW, Cerami A. 1980. Effect of various iron chelating agents on

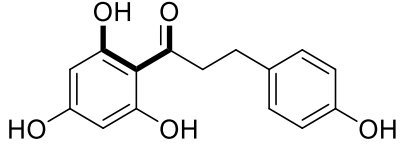
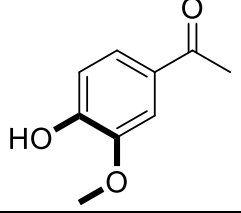
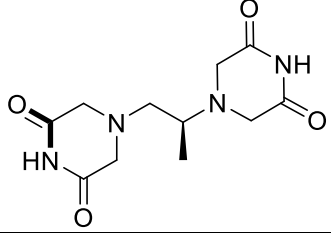
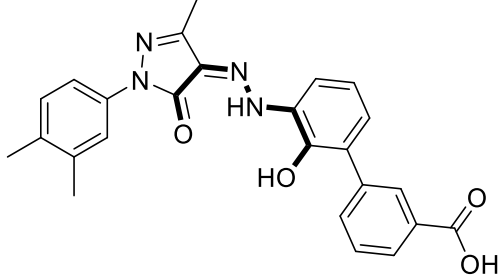
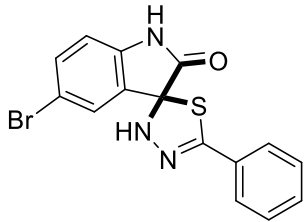
- 437 DNA synthesis in human cells. *Biochem Pharmacol* 29:1275–1279.
- 438 54. Shekhar-Guturja T, Gunaherath GMKB, Wijeratne EMK, Lambert JP, Averette AF, Lee SC, Kim T, Bahn
439 YS, Tripodi F, Ammar R, Döhl K, Niewola-Staszewska K, Schmitt L, Loewith RJ, P Roth F, Sanglard D,
440 Andes D, Nislow C, Coccetti P, Gingras AC, Heitman J, Gunatilaka Aal, ECowen L. 2016. Dual action
441 antifungal small molecule modulates multidrug efflux and TOR signaling. *Nat Chem Biol* 12:867–875.
- 442 55. Benvenisti-Zarom L, Chen J, Regan RF. 2005. The oxidative neurotoxicity of clioquinol.
443 *Neuropharmacology* 49:687–694.
- 444 56. Chitambar CR. 2017. The therapeutic potential of iron-targeting gallium compounds in human
445 disease: From basic research to clinical application. *Pharmacol Res* 115: 56-64.
- 446 57. De Léséleuc L, Harris G, KuoLee R, Chen W. 2012. In Vitro and in Vivo biological activities of iron
447 chelators and gallium nitrate against *Acinetobacter baumannii*. *Antimicrob Agents Chemother*
448 56:5397–5400.
- 449 58. Olakanmi O, Britigan BE, Schlesinger LS. 2000. Gallium disrupts iron metabolism of mycobacteria
450 residing within human macrophages. *Infect Immun* 68:5619–5627.
- 451 59. Wu J, Liu H, Zhang G, Gu L, Zhang Y, Gao J, Wei Y, Ma Z. 2016. Antileukemia effect of Ciclopirox
452 olamine is mediated by downregulation of intracellular ferritin and inhibition β -catenin-c-Myc
453 signaling pathway in glucocorticoid resistant T-ALL cell lines. *PLoS One* 11:e0161509.
- 454 60. Eberhard Y, McDermott SP, Wang X, Gronda M, Venugopal A, Wood TE, Hurren R, Datti A, Batey RA,
455 Wrana J, Antholine WE, Dick J, Schimmer AD. 2009. Chelation of intracellular iron with the antifungal
456 agent ciclopirox olamine induces cell death in leukemia and myeloma cells. *Blood* 114:3064–3073.
- 457 61. Vlachodimitropoulou E, Sharp PA, Naftalin RJ. 2011. Quercetin-iron chelates are transported via
458 glucose transporters. *Free Radic Biol Med* 50:934–944.
- 459 62. Van Acker SA b. e., Van Balen GP, Van Den Berg DJ, Bast A, Van Der Vijgh WJ f. 1998. Influence of
460 iron chelation on the antioxidant activity of flavonoids. *Biochem Pharmacol* 56:935–943.
- 461 63. Sharma S, Pal R, Hameed S, Fatima Z. 2016. Antimycobacterial mechanism of vanillin involves
462 disruption of cell-surface integrity, virulence attributes, and iron homeostasis. *Int J*
463 *Mycobacteriology* 5:460–468.

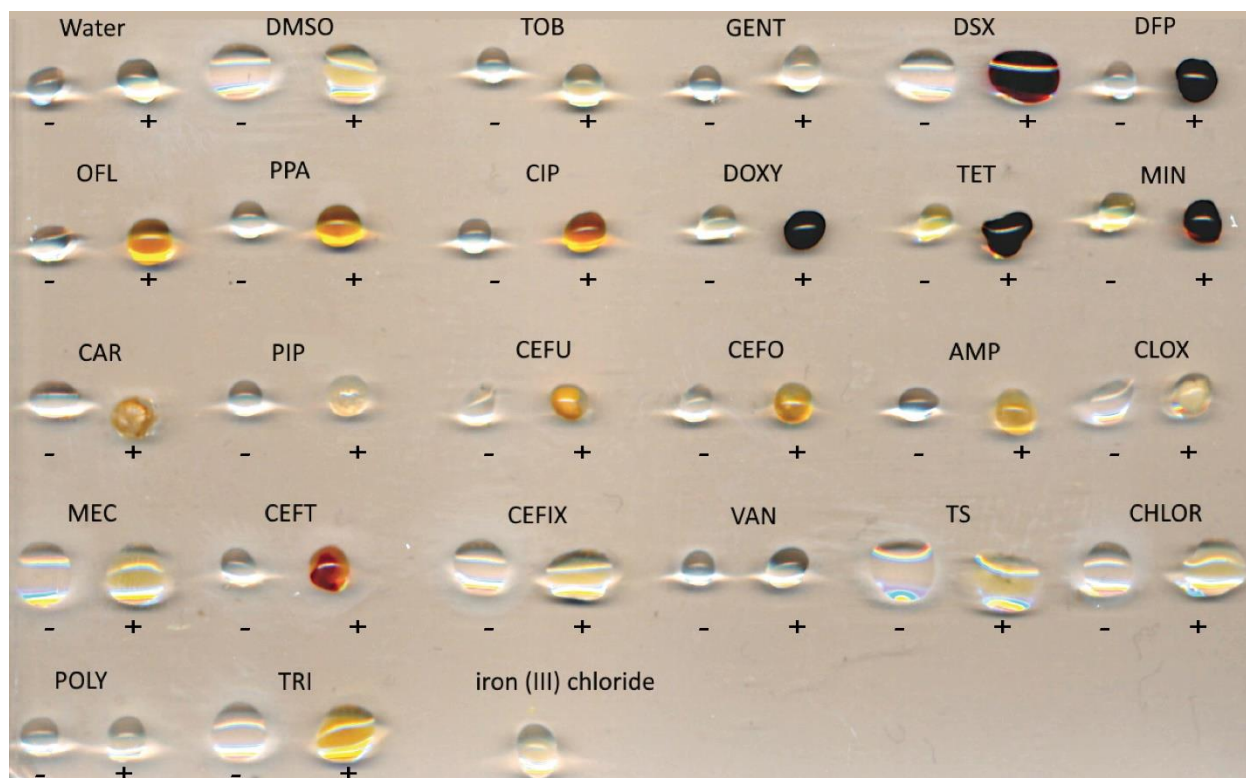
- 464 64. Hasinoff BB, Patel D, Wu X. 2003. The oral iron chelator ICL670A (deferasirox) does not protect
465 myocytes against doxorubicin. *Free Radic Biol Med* 35:1469–79.
- 466 65. Schroeder PE, Hasinoff BB. 2002. The doxorubicin-cardioprotective drug dexrazoxane undergoes
467 metabolism in the rat to its metal ion-chelating form ADR-925. *Cancer Chemother Pharmacol*
468 50:509–513.
- 469 66. Vlachodimitropoulou E, Chen Y-L, Garbowski M, Koonyosying P, Psaila B, Sola-Visner M, Cooper N,
470 Hider R, Porter J. 2017. Eltrombopag: a powerful chelator of cellular or extracellular iron(III) alone or
471 combined with a second chelator. *Blood* 130:1923–1933.
- 472 67. Bastian TW, Duck KA, Michalopoulos GC, Chen MJ, Liu ZJ, Connor JR, Lanier LM, Sola-Visner MC,
473 Georgieff MK. 2017. Eltrombopag, a thrombopoietin mimetic, crosses the blood–brain barrier and
474 impairs iron-dependent hippocampal neuron dendrite development. *J Thromb Haemost* 15:565–
475 574.
- 476 68. Roth M, Will B, Simkin G, Narayanagari S, Barreyro L, Bartholdy B, Tamari R, Mitsiades CS, Verma A,
477 Steidl U. 2012. Eltrombopag inhibits the proliferation of leukemia cells via reduction of intracellular
478 iron and induction of differentiation. *Blood* 120:386–394.
- 479 69. Falconer SB, Wang W, Gehrke SS, Cuneo JD, Britten JF, Wright GD, Brown ED. 2014. Metal-induced
480 isomerization yields an intracellular chelator that disrupts bacterial iron homeostasis. *Chem Biol*
481 21:136–145.
- 482

483 **Table 1:** The structures of literature-derived compounds used in this study with potential iron chelation
 484 sites bolded.

Compound	Structure	Description	Reference
Baicalin		Flavonoid isolated from the Chinese herb <i>Scutellaria baicalensis</i> with antioxidant, anti-inflammatory and anticancer activity.	(38–40)
Ferulic Acid		A natural product found in plant cell walls with antioxidant activity.	(41–43)
Sodium phytate		A naturally occurring compound found in wheat and rice with anticancer and antioxidant activity.	(44–46)
2,3,5,6-Tetramethylpyrazine		An alkaloid derived from the Chinese herb <i>Ligusticum wallichii</i> that is used to treat vascular diseases.	(41)

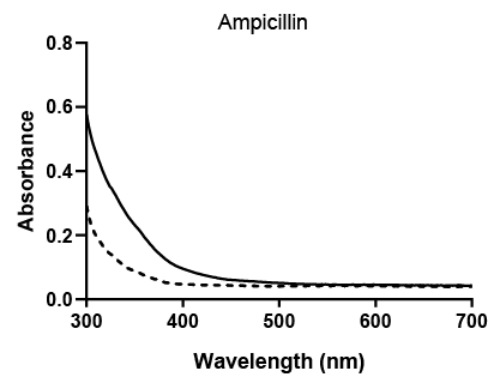
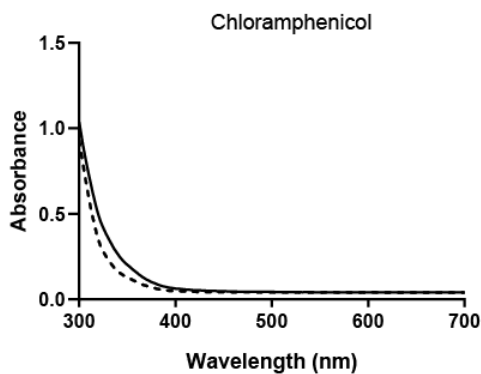
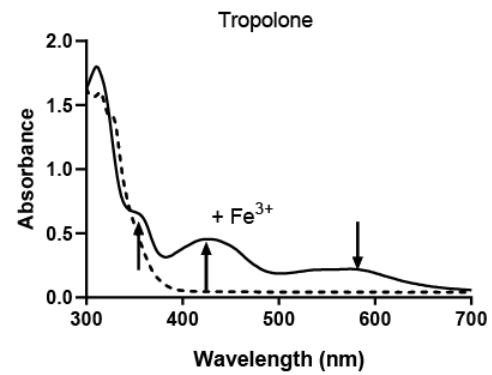
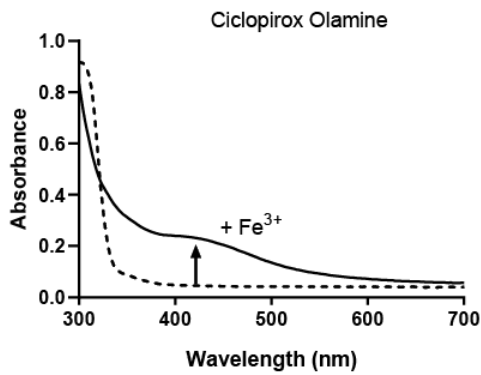
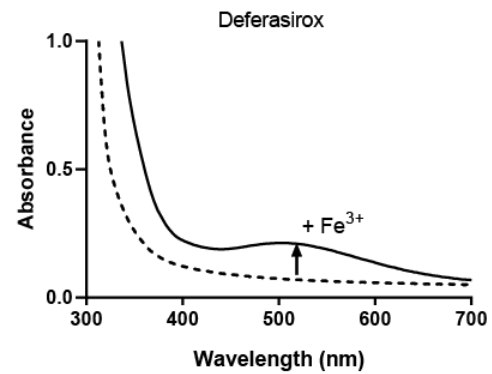
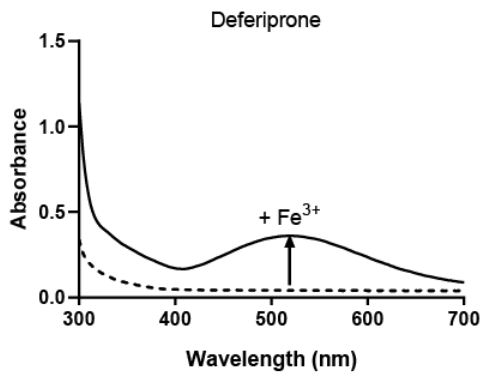
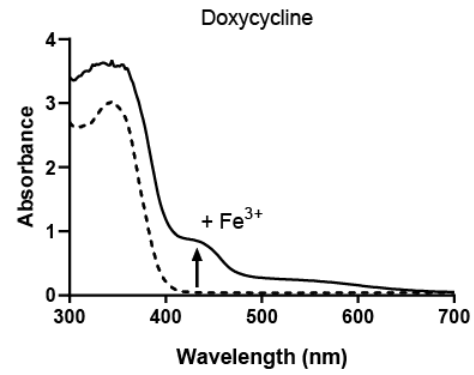
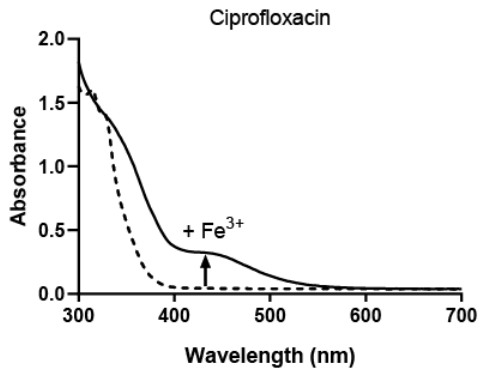
Curcumin		Natural product of turmeric with anticancer activity.	(47, 48)
Epigallocatechin Gallate		A polyphenol isolated from green tea extract.	(42, 49–51)
Tropolone		Synthetic compound with broad-spectrum antimicrobial activity.	(52, 53)
Clioquinol		Used to treat fungal and bacterial infections. Also used in the treatment of Alzheimer's Disease.	(40, 48, 54, 55)
Gallium Nitrate		Iron analogue with antimicrobial activity.	(56–58)
Ciclopirox Olamine		Antifungal agent.	(59, 60)

Phloretin		A flavonoid found in apples and pears.	(61, 62)
Apocynin		An NADPH-oxidase inhibitor.	(42, 63)
Dexrazoxane		Cardioprotective agent.	(64, 65)
Eltrombopag		A thrombopoietin receptor agonist used to treat thrombocytopenia.	(66–68)
Lipofermata		Fatty acid transport inhibitor.	(69)

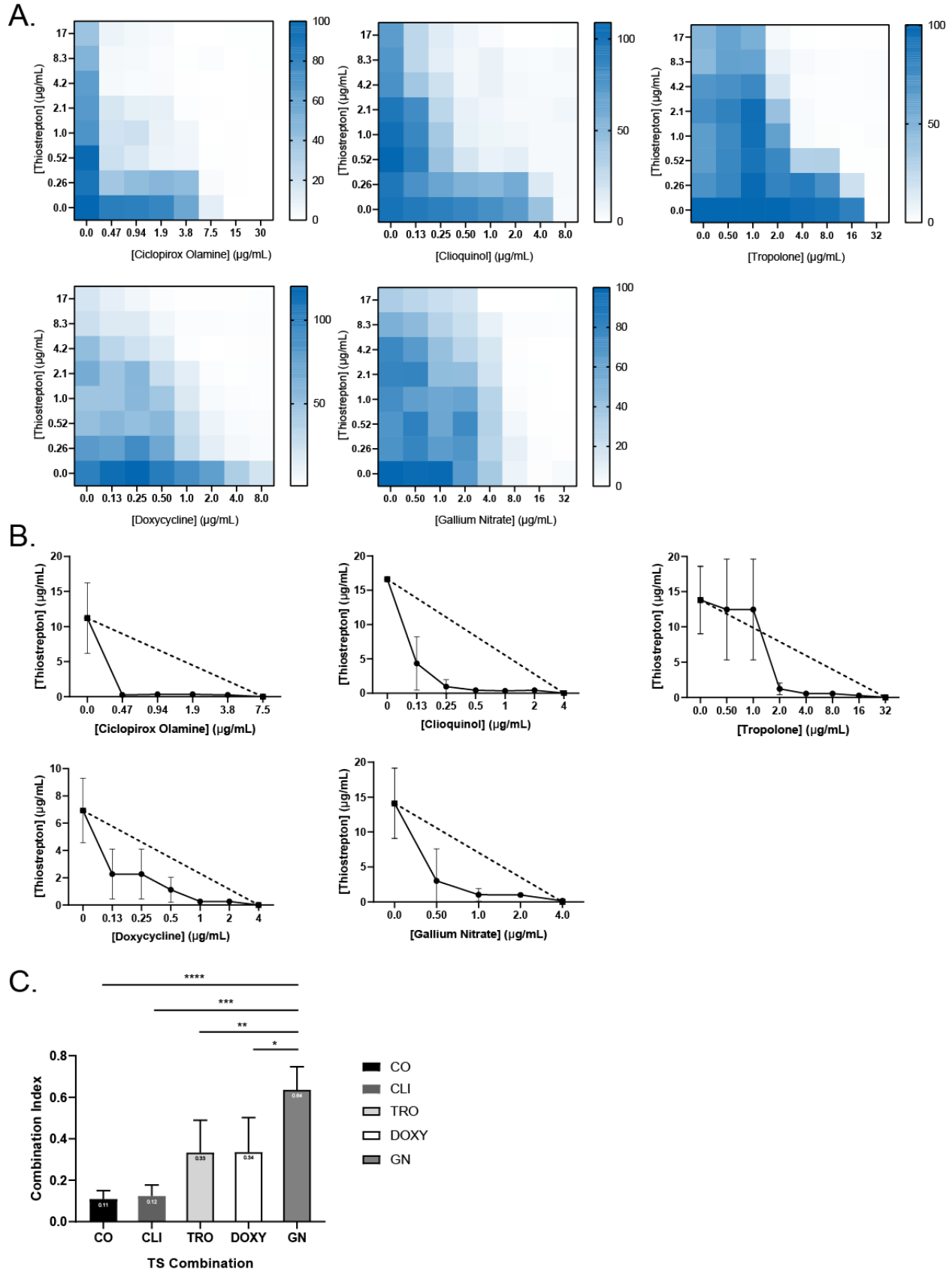


485

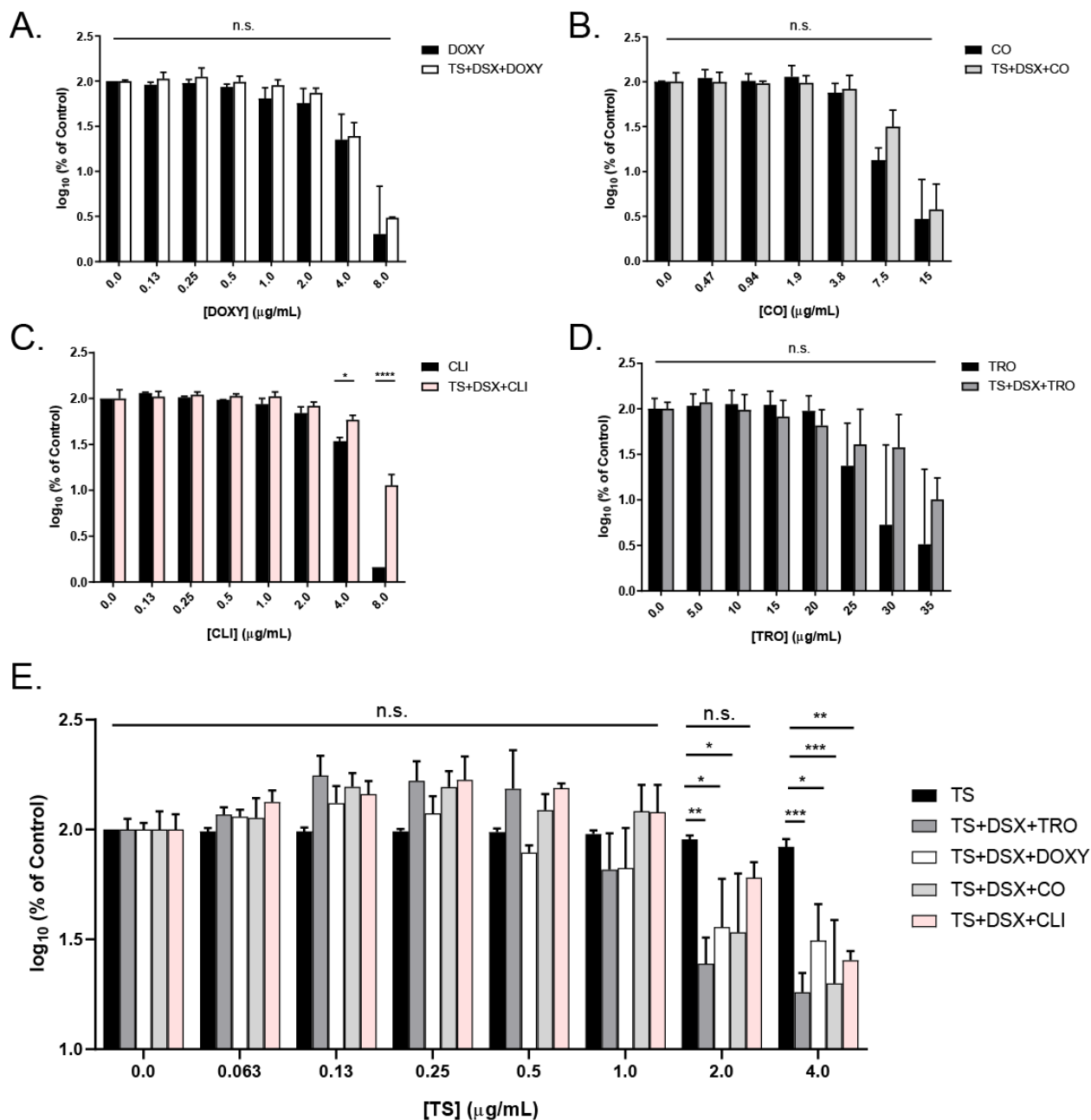
486 **Figure 1. Qualitative assay to identify potential antibiotic-Fe³⁺ complexes.** Binding of iron by a
487 compound causes spectral shifts that can be detected visually. Five μL of stock concentration antibiotic
488 (below) was added to $5\mu\text{L}$ of FeCl_3 to a final FeCl_3 concentration of $10\mu\text{M}$ and incubated at room
489 temperature for one hour. Negative controls without iron are indicated by a negative sign and droplets
490 with FeCl_3 are indicated with a positive sign. Vehicle controls with Milli-Q H_2O and DMSO were included.
491 The concentrations of each antibiotic stock were: TOB (tobramycin 4 mg/mL), GENT (gentamicin 10
492 mg/mL), DSX (deferasirox 20 mg/mL), DFP (deferiprone 60 mg/mL), OFL (ofloxacin 4 mg/mL), PIP
493 (piperacillin 64 mg/mL), CIP (ciprofloxacin 5 mg/mL), DOXY (doxycycline 50 mg/mL), TET
494 (tetracycline 20 mg/mL), MIN (minocycline 20 mg/mL), CAR (carbenicillin 100 mg/mL), PIPER (piperacillin
495 6 mg/mL), CEFU (cefuroxime 30 mg/mL), CEFO (cefotaxime 30 mg/mL), AMP (ampicillin 30 mg/mL),
496 CLOX (cloxacillin 30 mg/mL), MEC (mecillinam 30 mg/mL), CEFT (ceftriaxone 30 mg/mL), CEFIX (cefixime
497 12 mg/mL), VAN (vancomycin 30 mg/mL), TS (thiostrepton 20 mg/mL), CHLOR (chloramphenicol 50
498 mg/mL), POLY (polymyxin B 4 mg/mL), TRI (trimethoprim 50 mg/mL).



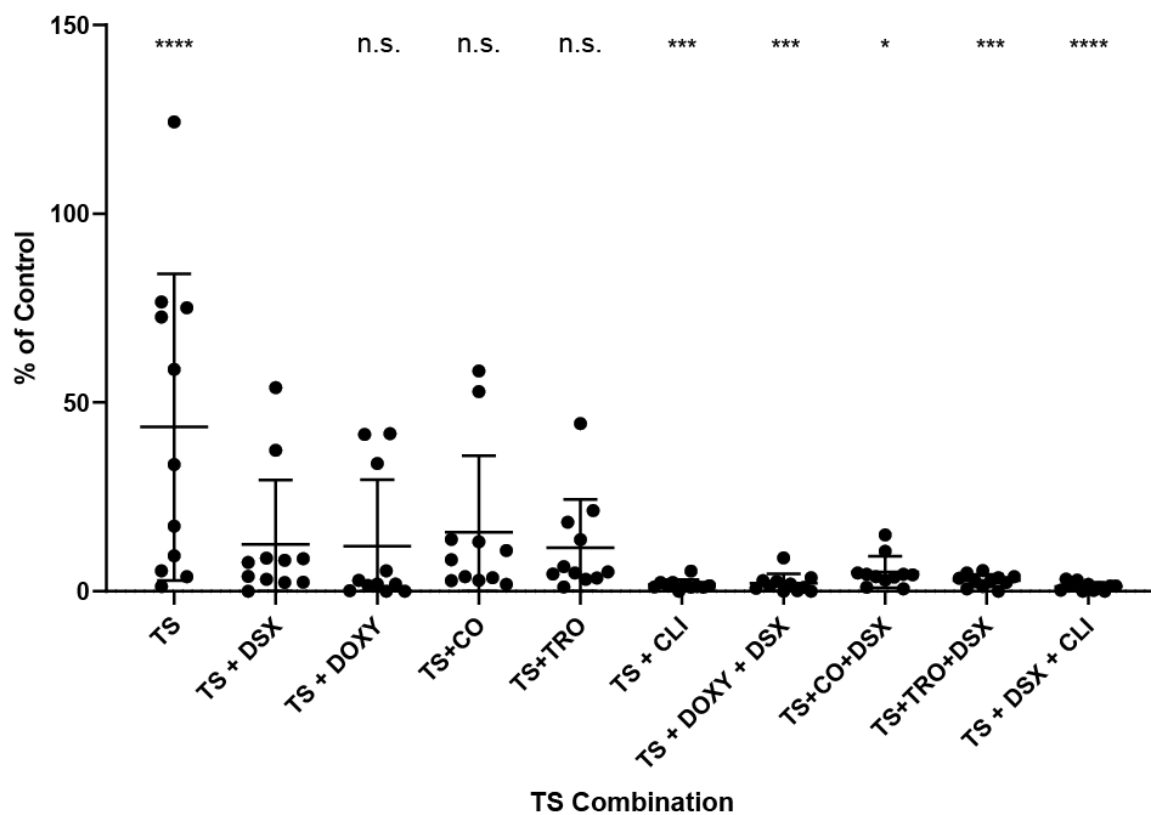
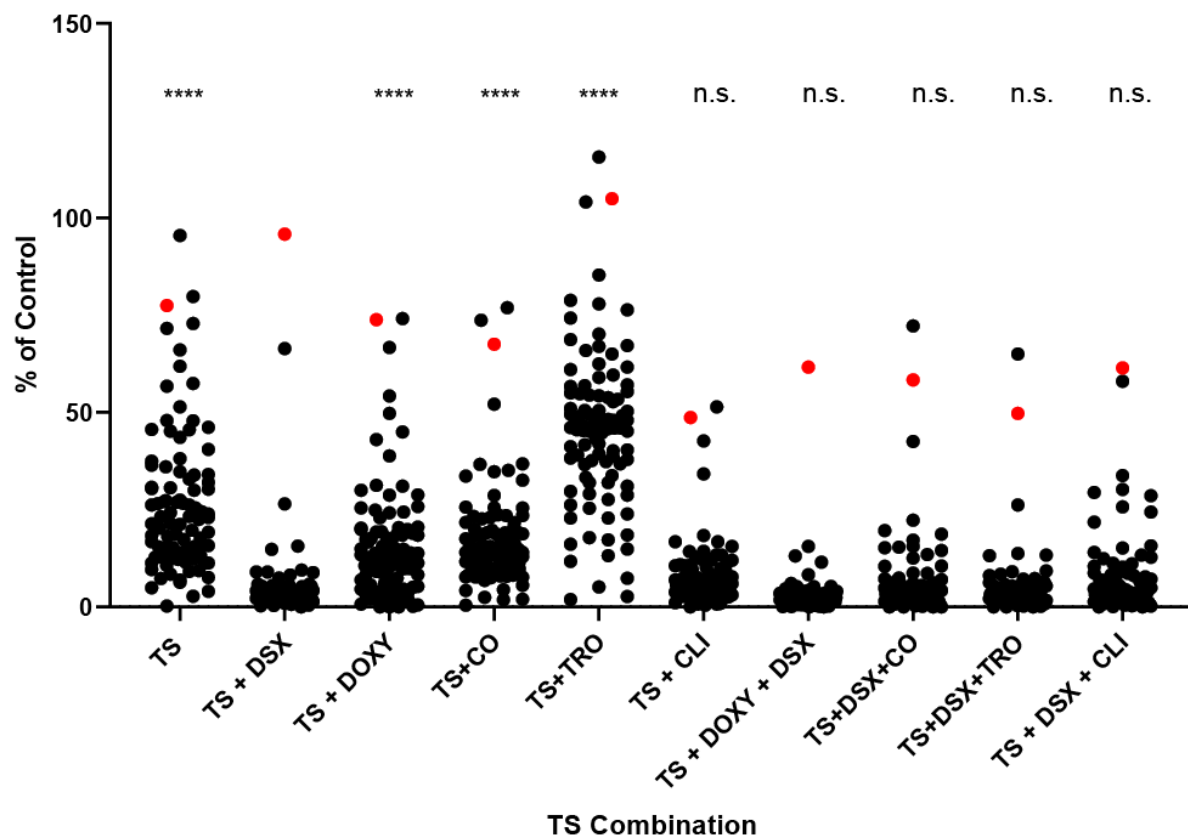
500 **Figure 2. UV-Vis absorption spectrum of compounds with and without Fe (III).** Equimolar
501 concentrations of compound and FeCl₃ were added in deionized H₂O to a final concentration of 300 μM
502 and a spectrum of wavelengths from 300 nm to 700 nm read after 1 h incubation at room temperature.
503 The black dashed line is the spectrum of the compound in the absence of iron. The black solid line is the
504 spectrum after the addition of iron. New peaks appearing after the addition of Fe³⁺ are indicated with
505 arrows. Chloramphenicol and ampicillin were used as negative controls. Each assay was performed at
506 least 3 times and averaged values are shown.



508 **Figure 3. Iron chelators are synergistic with TS against *P. aeruginosa* PA14. A.** Checkerboards and **B.**
509 IC₅₀ isobolograms are shown for each compound that synergize with TS. Dashed lines indicate the line of
510 additivity and solid lines indicate the IC₅₀ of TS at each compound concentration. Checkerboards and IC₅₀
511 isobolograms are arranged in the following order: CO, CLI, TRO, DOXY, and GN from left to right, top to
512 bottom. **C.** Combination indices (CI) of each TS combination. CI values are indicated at the top of the
513 bars. All experiments were conducted 3 times. Average values are reported. **** p<0.0001, ***
514 p<0.001, **, p<0.01.
515
516

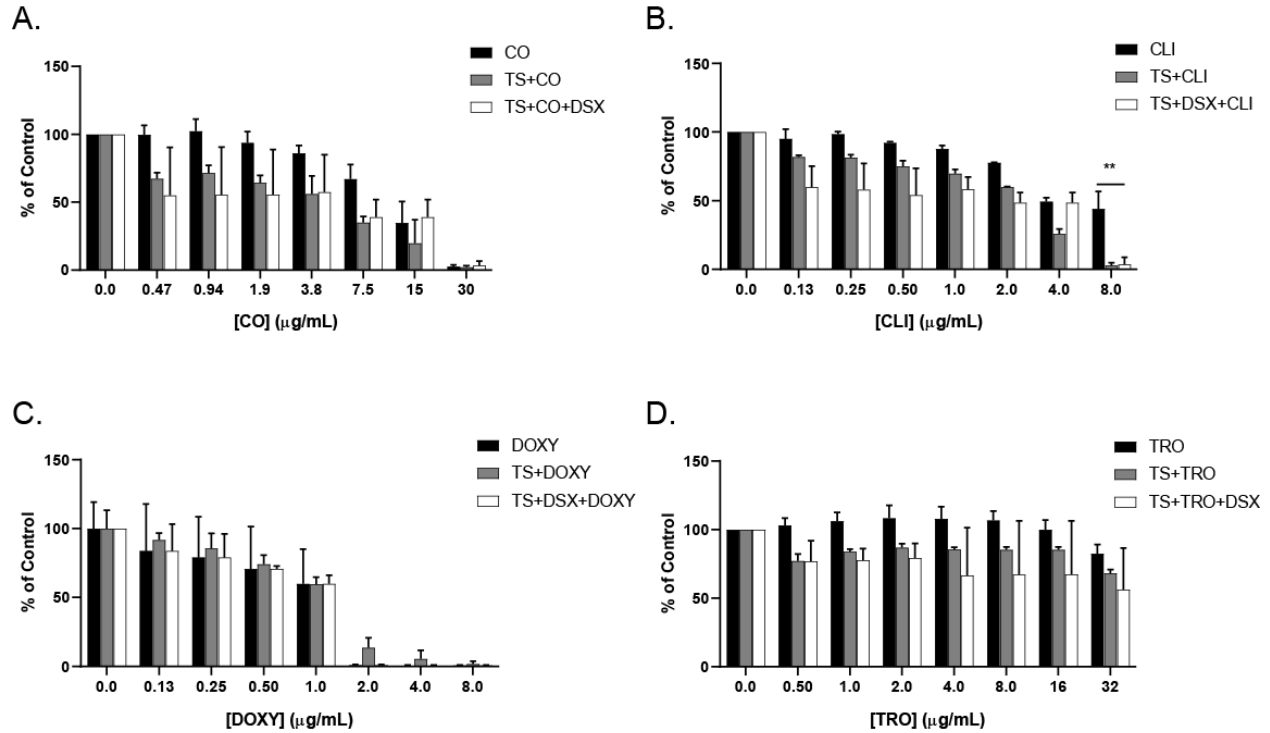


517
 518 **Figure 4. Unidirectional synergy between chelators and TS.** Surface areas of 3D checkerboards were
 519 plotted against chelator concentration in term of % of control on a \log_{10} scale and compared to the
 520 activity of each chelator alone. **A.** DOXY. **B.** CO. **C.** CLI. As shown in Figure S4, CLI antagonized with DSX
 521 against PA14, thus the triple combination allowed more growth than CLI alone at its highest
 522 concentration. However, the triple combination reduces growth below the previously established MIC,
 523 20% of control (21). **D.** TRO. **E.** Surface areas were graphed with respect to increasing TS concentrations
 524 and compared to the activity of TS alone. n.s., not significantly different. * $p < 0.05$, ** $p < 0.005$, ***
 525 $p < 0.0005$. The average of at least three biological replicates are shown.



527

528 **Figure 5. TS combinations inhibit the growth of clinical isolates.** Single, double, and triple TS
529 combinations were used to inhibit the growth of **A. *P. aeruginosa*** and **B. *A. baumannii*** clinical isolates.
530 Highly-resistant strain C0379 is highlighted in red. TS and DSX were used at 8.3 µg/mL and 32 µg/mL
531 respectively. The third compound was used at ¼ MIC against PA14 (1 µg/mL DOXY, 2 µg/mL CO, 4 µg/mL
532 TRO, and 1 µg/mL CLI). Horizontal bars show depict the mean % of control growth. Assays were
533 performed at least 3 times. Averaged values are shown. Statistics for TS + DSX versus TS alone or versus
534 other combinations are shown. n.s., not significantly different. *, p<0.05. ***, p<0.0005. ****,
535 p<0.0001.



536

537 **Figure 6. Growth of highly-resistant strain C0379 is inhibited with increased concentrations of CO, CLI,**
538 **and DOXY.** The resistant clinical isolate was challenged with single, double, and triple combinations of **A.**
539 **CO, B. CLI, C. DOXY, and D. TRO.** Increasing doses of each compound were combined with TS and DSX at
540 8.3 $\mu\text{g/mL}$ and 32 $\mu\text{g/mL}$, respectively. MIC assays were conducted at least 3 times and averaged results
541 are shown. **, $p < 0.001$.